2017

TECHNICAL REPORT

UNIVERSITY OF Hull

COMPARING THE EFFECT OF ROTOR SIZING VERSUS ROTOR SPEED ADJUSTMENT ON CENTRIFUGAL COMPRESSOR ENERGY REQUIREMENT FOR CO_2 PIPELINE TRANSPORTATION

AUTHOR:

CHIMAOGE .N. OKEZUE

RESEARCH SUPERVISOR:

DMITRIY KUVSHINOV

INSTITUTION:

THE SCHOOL OF ENGINEERING AND COMPUTER SCIENCE
UNIVERSITY OF HULL

JULY 2017

ABSTRACT

At the design stage of pipeline networks, it is common for engineers to include a margin of safety in sizing compressors to account for future expansions in system capacity. In the context of carbon capture and storage (CCS), this margin of safety is extended to account for changes in the purity of the supercritical carbon dioxide working fluid because of its effect on compressor energy requirement. However, when deciding on a margin of safety, it is not always possible to anticipate all the variations that will occur in the chemical composition of the working fluid over a long period of time. So it may be inevitable that over a long period of time, the energy requirement of a compressor will rise beyond what was originally anticipated due to significant changes in the composition of the impure CO_2 stream caused by alteration in capture technology or type of fuel burned in a power plant connected to the transport pipeline. Nevertheless, savings can be made in operating costs, if compressor performance can be optimized.

When the composition of the CO_2 stream changes, the minimum operating pressure required to maintain that fluid in supercritical phase inside the pipeline changes as well. In order to meet the required minimum operating pressure, the compressor rotor speed will either have to be increased or the machine can be re-sized while rotor speed remains constant. Either way, an increase in energy requirement is unavoidable. Increasing the rotor speed while machine size remains unchanged will incur higher energy losses than a proportional increment in machine size while keeping rotor speed constant. Despite this fact, in pipeline engineering, it is common practice to adjust compressor's rotor speed to maintain the minimum operating pressure because it is easier than re-sizing the compressor's rotor.

As a prerequisite for developing a procedure for optimizing centrifugal compressor performance, it is vital that the effect of increasing the machine's speed be analyzed and compared against the effect of increasing its size. To this end, a quasi-dimensional model based on the laws of conservation was developed in MATLAB® to compare the effect of re-sizing the rotor against the effect of adjusting its speed on the energy requirement of a compressor handling supercritical carbon dioxide of varying chemical purity. Results of the study demonstrate that the performance of a compressor is affected by the impurities in the CO_2 stream. Moreover, the study confirms that it is more cost-effective to increase compressor's rotor size while the rotor speed remains constant than vice-versa.

Keywords: *CCS transport; compressor performance curve; energy requirement; working fluid; impurities; CO_2 pipeline; quasi-dimensional model; pump; compressor; supercritical phase; critical point; equation of state; laws of conservation*

Nomenclature

A	Area [m^2]
b	Impeller width
d, D	Diameter [m]
dF	Change in Force [N]
f	Fanning's Friction Factor [–]
Gap	Width of clearance between Impeller and compressor housing [m]
h	Specific Enthalpy [kJ/kg]
H	Height [m]
K	Loss Coefficient [–]
L	Characteristic Length [m]
$\dot{m}$	Mass Flow Rate [kg/s]
n_B	Number of Impeller Blades [–]
N	Rotor Shaft Speed [rpm]
P	Pressure [bar]
r	Radius [m]
Re	Reynolds Number [–]
s	Specific Entropy [kJ/kgK]
S_F	Slip Factor [–]
T	Temperature [K]
U	Impeller blade tip speed [m/s]
V	Velocity [m/s]
W	Specific Work [kJ/kg]

Greek Symbols

β	Impeller Blade Angle
Δ	Finite Difference [–]
μ	Viscosity [mPa.s]
ρ	Fluid Density [kg/m^3]
θ	Wrap Angle [deg]
ϕ	Convergence Angle [deg]
η	Efficiency [–]
π	Pi Constant [–]
ω	Angular Speed [rad/s]
τ	Shear Stress [Pa]

Subscripts

1	Compressor Inlet (Suction); leading edge of impeller
2	Compressor Outlet (Discharge); trailing edge of impeller
a	Actual Value
ave	Average Value
con	Converging Duct
crit	Critical Value
curv	Curved Surface
disk	Disk Friction

euler	Ideal Value
gap	Impeller Tip Leakage Channel
HYD	Hydraulic Value
i	Root of Impeller Eye
IMP	Impeller
INPUT	Actual Input Value
ISEN	Isentropic Value
leak	Leakage
loss	Loss
m	Meridional Direction
o	Tip of Impeller Eye
rad	Radial Coordinate
rel	Relative Value
sum	Sum of Values
t	Tangential Coordinate

1. Introduction

In pipelines, CO_2 can be transported in gaseous, liquid, dense or supercritical states. CO_2 is in dense phase (also called “dense-liquid phase”) when its pressure is above the critical point while its temperature remains below the critical point. Supercritical CO_2 occurs when both temperature and pressure are above critical point (73.76 bar; 30.97°C) [1-3]. CO_2 stream in dense or supercritical state have high density close to that of liquid CO_2 and low viscosity close to that of gaseous CO_2. This means that a larger amount of CO_2 per unit time can be transported in supercritical state than in gaseous or liquid state with low pipeline frictional pressure drop per unit mass (since viscosity is quite low). Therefore, from an economic standpoint, CO_2 is best transported in long distance pipelines when in dense or supercritical phase [1-4]. Moreover, cavitation and surging which can damage compressors and pumps are impossible when CO_2 stream is above the critical point [5].

A typical CO_2 transport pipeline network consists of pipes, valves, compressors and booster pumps. Compressors are used to pressurize CO_2 beyond its critical point and booster pumps are required to ensure that the operating pressure inside the transport pipeline does not drop below the critical pressure of CO_2.

Anthropogenic CO_2 which the pipelines are intended to transport tends to contain chemical impurities such as CH_4, H_2, H_2O, H_2S, N_2, CO, O_2 and Ar. These impurities, even in trace amounts, can substantially alter the normal thermodynamic properties of CO_2 such as phase behaviour, compressibility, density, enthalpy, pressure, temperature and viscosity, thereby significantly affecting the general performance of the pipeline network [6-12]. As shown in Figs.1 (a) and 1(b), certain types of impurities can reduce the overall fluid density while increasing the critical point of CO_2 resulting in a high energy requirement for the compressors and pumps [7-12].

Impurities can also enlarge the two-phase region in the CO_2 phase envelope depicted in Fig.1 (a), increasing the risk of single-phase supercritical fluid transforming into a gas-liquid two-phase fluid if there is a slight pressure drop in the pipeline. Since compressors and pumps are part of the pipeline network, the formation of two-phase flow can lead to cavitation which may potentially damage both machines. To avoid this particular risk, the pipeline operating pressure will have to be very high, far beyond the critical pressure of the impure CO_2 stream. Higher pressures lead to higher energy requirement for the compressor and pumps, resulting in even greater operating costs for the pipeline network [12, 14].

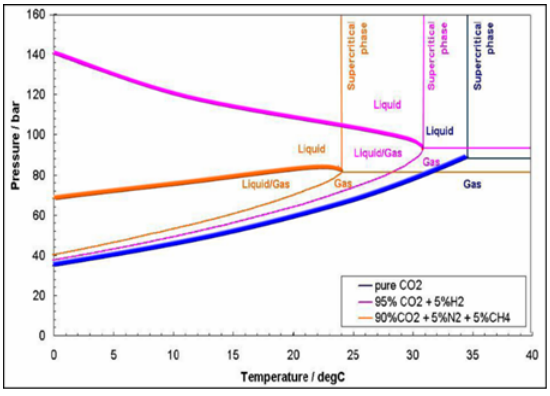

Fig. 1(a). Effect of impurities on the phase envelope [39]

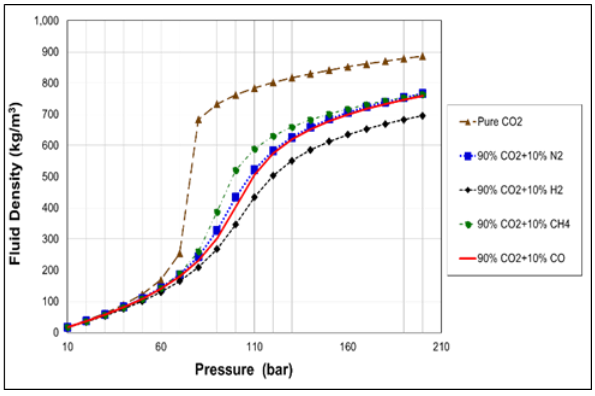

Fig. 1(b). The effect of impurities on density of CO2 at 305 K

A lot of research studies have been published on CO_2 pipeline transport covering design issues such as pipeline sizing, recompression distance, energy requirement, corrosion and fracture propagation [7-15] and operational issues such as start-up, shut-down, rapid depressurization, valve blockage and variation of fluid flow rate [15-18]. In many of these studies, compressors and pumps are not analyzed in great depth because normally the focus is on a globalized evaluation of the entire transport pipeline network rather than a localized analysis of individual key components within the network.

Studies [4, 19, 20] have compared several multi-stage centrifugal compressors of different configurations in a CO_2 pipeline network to determine the one with the least energy requirement. Although they provide important information on energy requirement of compressors under various operating conditions, the models they use are not adequately detailed to be used for appropriate sizing and selection of these machines. In these models, fluid compression is simulated with adiabatic or polytropic process equations which neglect the geometry and internal fluid flow processes within these machines. Moreover, in both process equations, the compressor efficiency is assumed to be fixed. Where as in reality, machine efficiency varies with the concentration and the type impurities present in the CO_2 stream [21].

Compressors and pumps consume most of the energy required to operate an entire CO_2 pipeline network. According to Moore et al. [22], the energy consumed by pure CO_2 compression in a CCS facility connected to a power station can reduce the overall efficiency of that station by 8-12%. The energy penalty is even greater if the CO_2 stream involved contains certain impurities. Therefore, it is vital that an optimal procedure for compressor sizing and selection be developed to ensure that machines with the best attainable efficiency per power utilized are installed in the pipeline network to reduce this energy penalty and save operating costs.
In the context of Carbon Capture and Storage (CCS), available compressor performance curves are not adequate for this purpose as none has been developed for impure CO_2 streams at supercritical or dense phase conditions. This study tackles this significant gap in knowledge by developing a quasi-dimensional model incorporating centrifugal machine geometry and using it to compare the effect of rotor re-sizing against the effect of rotor speed adjustment on the work input required for a compressor handling supercritical carbon dioxide of varying chemical purity.

2. Selecting Equations of State for CO_2 Property Calculation

Equations of State (EoS) correlations provide the underpinning mathematical relationship between the pressure, volume, temperature and composition of a chemical substance. In the context of CCS, these correlations are necessary for calculating CO_2 thermodynamic properties such as enthalpy, density and viscosity which are needed as inputs for hydraulic equations used in describing flow of CO_2 stream at supercritical or dense phase conditions. However, in the vicinity of the critical point, a slight change in pressure or temperature can engender in a large change in aforementioned CO_2 properties. This makes accurate CO_2 property calculation difficult when transported in supercritical or dense phase conditions [3, 23, 24, 25]. When impurities are present in the CO_2 stream, the difficulty in property calculation is further exacerbated.

Reliable calculation of the CO_2 properties is essential for the cost-effective design and operation of CO_2 transport pipeline network [6, 26]. Accurate prediction of density and pressure drop is necessary for designing compressors and pumps [27] or facilitating correct sizing and selection of ready-made compressors and pumps [28].

Given their importance, several types of EoS correlations namely Peng-Robinson (PR), Soave-Redlich-Kwong (SRK), Benedict-Webb-Rubin (BWR), Lee-Kessler (LK), Statistical Associating Fluid Theory (SAFT), Span and Wagner (SW) published in open literature have been analysed by various authors and while no single correlation can perform satisfactorily for all thermodynamic conditions, some correlations will perform better than others under certain conditions [4, 7]. For instance, the highly complex Span and Wagner (SW) correlation produces highly accurate results when the CO_2 stream is pure, but difficult to extend to CO_2 stream containing impurities [29, 30]. Peng-Robinson (PR) correlation is widely used because of its compelling simplicity, but has been found to be inaccurate at supercritical and dense phase conditions [29]. Demetriades et al. [29] proposed a new EoS that can predict the properties of pure CO_2 at dense phase condition with the simplicity of PR and accuracy of SW and extended it in [31] to include CO_2 in binary mixtures with N_2, O_2 and H_2. While this new EoS shows promise, it still remains under development and yet to be validated extensively.

GERG and SAFT equations of state (EoS) has shown better potential for accurate prediction of properties of impure CO_2 mixtures [30, 32]. However, despite its high level of accuracy, SAFT-based EoS has not been studied and developed sufficiently for use in modelling CCS transport pipeline at dense or supercritical phase conditions [4]. On the other hand, GERG-2004 is the international reference EoS for natural gas, which has been applied successfully by researchers such as [10, 11, 15, 16, 18] in calculating CO_2 properties for pipeline transport models over a range of conditions relevant to CCS.

In this study, the highly accurate Span and Wagner (SW) EoS is used for property calculations involving pure CO_2 while GERG-2008, an improved variant of GERG-2004, is used to calculate impure CO_2 mixture properties. GERG-2008, gives accurate results for natural gas mixtures from low pressures to high pressures of up to 300 bar [33] and temperatures above 290 K [32] which fits perfectly within the boundaries of operational conditions of a small compressor simulated with the proposed mathematical model.

3. Model Development & Validation

3.1 Modelling Strategy

Traditionally, fluid compression is modelled as an adiabatic or polytropic process based on ideal gas assumptions [11, 15, 19, 20]. When corrected to account for the fact that the working fluid is real rather than ideal, this traditional modelling strategy works reasonably well. However, this type of model excludes the internal fluid process and geometry of the compressor and therefore is unsuitable for compressor selection and sizing.

Adiabatic and polytropic process equations calculate energy requirement of compressors handling impure CO_2 at conditions near the critical point under the assumption that isentropic efficiency is fixed regardless of the working fluid's chemical composition. However, studies carried out by Okezue and Wang [21] showed that the isentropic efficiency is not

fixed and can vary quite significantly if the concentration of certain impurities (e.g. hydrogen) in the CO_2 stream is high.

The quasi-dimensional model proposed in this study does not assume that the isentropic efficiency is known apriori. So the effect of various impurities on compressor isentropic efficiency can be studied with this model.

Wright et al. [23], Lee et al. [24, 34] and Aritomi et al. [25] reported significant errors in the calculation of isentropic efficiency when enthalpy values obtained from EoS correlations were used. This can be attributed directly to the difficulties EoS correlations encounter when working at the vicinity of the critical point. EoS correlations generate much lower errors when predicting density compared to when predicting enthalpy and specific heat capacity [34].

Therefore, the modelling strategy adopted in this study seeks to minimize the role of EoS correlations (especially in predicting enthalpy) where possible. For instance, energy requirement is calculated in the proposed model using information on machine geometry and rotor shaft speed, thereby limiting the role of EoS property calculation to providing just fluid density data. Enthalpy calculation is not required for predicting compressor work input and isentropic efficiency in this study.

3.2 Governing Equations

The proposed quasi-dimensional model is governed by steady-state mass and energy conservation equations. All model equations are implemented in MATLAB® and describe the physics of a centrifugal machine (See Fig. 2).

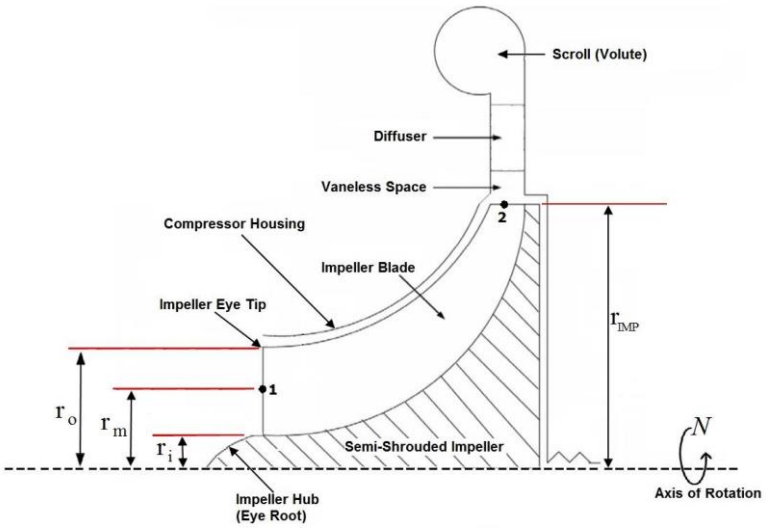

Fig.2. Meridional (sectional) view of a centrifugal compressor

3.2.1 Mass Conservation Law

Mass balance of the working fluid using a centrifugal compressor as control volume gives:

$$\left.\frac{dm}{dt}\right|_{cv} = \dot{m}_2 - \dot{m}_1 = 0 \qquad (1)$$

For the inlet (i.e. suction) side of the compressor:

$$V_1 = \frac{\dot{m}}{\rho_1 A_1} \tag{2}$$

$$\rho_1 = \Psi\left(\mathrm{P}_1, \mathrm{T}_1\right) \tag{3}$$

$$A_1 = \frac{\pi\left(d_o^2 - d_i^2\right)}{4} \tag{4}$$

$$b_1 = \frac{\left(d_o - d_i\right)}{2} \tag{5}$$

Ψ = function symbol

where, $\dot{m}, V_1$, A_1, b_1, and ρ_1 represent the actual fluid mass flow rate, axial component of the inlet fluid velocity, inlet flow area, width of impeller at the leading edge and inlet fluid density, respectively. The inlet fluid density is calculated with an EoS correlation using inlet pressure (P_1) and inlet temperature (T_1). The inlet flow area is an annulus formed by the concentric gap between the diameters of the eye tip (d_o) and eye root (d_i) of the impeller rotor.

$$\mathrm{U}_1 = \frac{\pi N\left(d_o^2 + d_i^2\right)}{120} \tag{6}$$

As soon as the compressor shaft starts spinning at a particular rotational speed (N), tip speeds are developed at the leading and trailing edges of the impeller blades. The tip speed at the impeller's leading edge (U_1) is the average of the peripheral speeds at the tip and root of the impeller eye. The rotating blades impacts angular momentum to the working fluid flowing in from the inlet. However, the tangential component of the inlet fluid velocity (V_{t1}) is less than blade tip speed (U_1) owing to flow separation and formation of eddies.

$$\mathrm{V}_{\mathrm{t1}} = \mathrm{U}_1 \times S_F \tag{7}$$

The slip factor (S_F) defines the "slip" or the deviation of V_{t1} from U_1 and is expressed mathematically using the equation developed by Stodola [35]. It is important to note that V_{t1} only exists if there are internal guide vanes (IGV) at the compressor inlet to channel the axial inflow of the working fluid around the circumference of the blades. For compressors that have no IGV, the value of V_{t1} is simply zero.

$$\mathrm{V}_{\mathrm{rel1}} = \sqrt{\mathrm{V}_1^2 + \left(\mathrm{U}_1 - \mathrm{V}_{\mathrm{t1}}\right)^2} \tag{8}$$

The inlet relative velocity (V_{rel1}) at which the working fluid enters the impeller eye can be solved using Pythagoras's theorem since it is one side of a right-angled vector triangle while U_1, V_1 and V_{t1} form the remaining sides.

On the outlet (i.e. discharge) side of the compressor:

$$\rho_2 = \frac{\dot{m}}{V_{rad2} A_2} \tag{9}$$

$$A_2 = \pi D_{IMP} b_2 \tag{10}$$

$$U_2 = \frac{\pi D_{IMP} N}{60} \tag{11}$$

$$V_{t2} = U_2 \times S_F \tag{12}$$

$$V_2 = \sqrt{V_{rad2}^2 + V_{t2}^2} \tag{13}$$

$$V_{rel2} = \sqrt{V_{rad2}^2 + \left(U_2 - V_{t2}\right)^2} \tag{14}$$

where ρ_2, A_2, D_{IMP}, b_2, U_2, V_{t2}, and V_{rad2} represent the outlet fluid density; outlet flow area; impeller blade diameter; width of impeller at the trailing edge; tip speed at the impeller's trailing edge; tangential component and the radial component of the exit fluid velocity, respectively. V_{rad2} is assumed to be approximately equal to V_1 as recommended by Saravanamutto et al. [36]. The vector sum of the radial component (V_{rad2}) and tangential component (V_{t2}) is the absolute exit velocity (V_2). On the other hand, V_{rel2} is the relative exit velocity.

3.2.2 Energy Conservation Law

Performing a specific energy balance of the working fluid using in a centrifugal compressor as the control volume, yields equation (15) which can be used to obtain the actual exit enthalpy of the fluid at the discharge of the compressor:

$$h_{2a} = \left(h_1 + \frac{V_1^2}{2} + W_{INPUT} \right) - \frac{V_2^2}{2} \tag{15}$$

As mentioned earlier, the modelling strategy adopted in this study seeks to minimize the role of EoS correlations where possible. Nevertheless, there are cases where the major use of the EoS is unavoidable. Inlet enthalpy (h_1) for equation (15) is calculated with the EoS correlations using inlet pressure (P_1) and inlet temperature (T_1).

$$T_2 = \Psi\left(P_2, h_{2a}\right) \tag{16}$$

While the actual outlet temperature (T_2) of the working fluid is calculated with the EoS using outlet pressure (P_2) and the actual outlet enthalpy (h_{2a}) as shown in equation (16).

In the field of turbomachinery, the traditional method of calculating energy of the working fluid within a centrifugal compressor or pump is to use the Euler equation (17) as expressed in [36, 37]. However, equation (17) does not include any energy losses (frictional or otherwise) and therefore is not the actual energy (W_{INPUT}) supplied to compressor's rotating

impeller blades. It is the ideal energy (W_{euler}) that will be impacted to the fluid if we assume compressor operation is frictionless (i.e. compression is an isentropic process).

$$W_{euler} = \frac{1}{2}\left[\left(V_2^2 - V_1^2\right) + \left(U_2^2 - U_1^2\right) + \left(V_{rel2}^2 - V_{rel1}^2\right)\right] \quad (17)$$

It is common practice to calculate the actual energy input (W_{INPUT}) by dividing ideal energy (W_{euler}) with an assumed isentropic efficiency (η_{ISEN}). The problem with this methodology is that the same isentropic efficiency is used regardless of the composition of the CO_2 mixture flowing inside the compressor. Yet it is known that variation in efficiency can be significant if the concentration of certain impurities in the supercritical CO_2 mixture is high [21].

$$W_{INPUT} = W_{euler} + \sum W_{losses} \quad (18)$$

$$\eta_{ISEN} = \frac{W_{euler}}{W_{INPUT}} \times 100\% \quad (19)$$

In the proposed model, W_{INPUT} is calculated from its fundamental definition—the sum of the ideal work input (W_{euler}) and energy losses (both internal and external) as shown above. These losses ($\sum W_{losses}$), which are modelled in great details in the section 3.2.3, include disk frictional losses, hydraulic losses and leakage losses. Isentropic efficiency (η_{ISEN}) is calculated with equation (19).

$$\int dh = \int Tds + \int \frac{dP}{\rho} \quad (20)$$

$$\Delta h_{ISEN} \approx \frac{\Delta P}{\rho_{ave}} \approx W_{euler} \quad (21)$$

$$P_2 \approx P_1 + \frac{\rho_{ave}}{2}\left[\left(V_2^2 - V_1^2\right) + \left(U_2^2 - U_1^2\right) + \left(V_{rel2}^2 - V_{rel1}^2\right)\right] \quad (22)$$

Equations (20) to (22) describes how the discharge pressure of the compressor (P_2) is calculated by combining the first law of thermodynamics for an isentropic process ($Tds = 0$) and the equation for energy requirement for an ideal (i.e. frictionless) compressor. Δh_{ISEN} is a close approximation of the isentropic enthalpy change while ΔP and ρ_{ave} are the differential pressure and the average of the inlet and outlet fluid densities, respectively.

3.2.3 Modelling Energy Losses

As shown in equation (18), the actual compressor work input consists of two parts– ideal work done on the fluid by impeller blades (W_{euler}) and the energy losses. There are several sources of energy losses in a centrifugal machine.

They can be broadly split into two categories namely, internal and external losses. Energy losses in the flow path of the working fluid inside the compressor is categorized as “Internal losses”. Examples of this kind of losses are disk friction loss (W_{disk}), leakage loss (W_{leak}) and hydraulic loss (W_{HYD}). Energy dissipation due to skin contact between exterior components of

the compressor are called “external losses”. Examples of external losses are mechanical losses in bearings and seals of the compressor shaft.

The external losses are far much smaller than internal losses. Considering that many modern centrifugal machines today have rotor shafts supported by low friction magnetic or gas bearings, it is reasonable to ignore external losses in the compressor models. In this study, the energy losses in the compressor is restricted to internal losses alone as shown in equation (23).

$$\sum W_{losses} \approx \; W_{disk} + W_{leak} + W_{HYD} \tag{23}$$

3.2.3.1 Disk Friction Loss

The rotation of the impeller in the working fluid generates shear stresses between its moving exterior surfaces and the stationary interior walls of the compressor housing. Some of the energy supplied to the compressor is lost in overcoming friction associated with these shear stresses which is heavily dependent on the fluid density, shaft speed and impeller size. In the context of CCS transport, this source of energy loss can be quite significant considering the high compressor speeds and large fluid densities of supercritical CO_2 based working fluids involved.

$$W_{disk} = W'_{disk} + W''_{disk} \tag{24}$$

The profile of shear stresses generated on the exterior surface of the rotating impeller runs frontally from the hub to the circumference and the back of the rear shroud. In order to develop a simplified mathematical expression for the disk friction energy loss, the complex shape of the semi-shrouded impeller is simplified by assuming that it is a combination of a disc plate and frustum. In effect, the disk friction loss is modelled as the sum of energy loss on disc rotating in the working fluid ($\dot{W}'_{disk}$) and energy loss on the curved surface of a conical frustum ($\dot{W}''_{disk}$) as shown in equation (24).

$$W'_{disk} = \frac{1}{\dot{m}} \int \omega r dF = \frac{1}{\dot{m}} \int \omega r \left(\tau dA\right) = \frac{1}{\dot{m}} \int \pi \rho f_{disk} \omega^3 r^4 dr \tag{25}$$

Energy loss on the disc plate ($\dot{W}'_{disk}$) is approximate to the actual disk friction loss on the back surface of the rear shroud of the impeller. As shown in equation (25), $\dot{W}'_{disk}$ is a function of the angular speed (ω) of the impeller and the torque of the rotor shaft, a product of the impeller radius (r) and the change in force along the profile of the rear shroud (dF). Shear stress (τ) arises from the force vector acting parallel to the external surface of rear shroud and the inner surface of the compressor housing. The actual mass flow rate of fluid flowing out of compressor discharge port is represented by ($\dot{m}$).

The local friction factor corresponding to the shear stresses on the smooth surface of the disc plate is calculated using a modified version of the Blasius correlation for turbulent flows as shown in equation (26) below:

$$f_{disk} = 0.046\left(\mathrm{Re}\right)_{disk}^{0.20} \tag{26}$$

The approximate Reynolds Number (Re_{disk}) for the disc plate is presented in equation (27):

$$\mathrm{Re}_{disk} \approx \frac{\rho_2 U_2 \left(D_{IMP} - d_i\right)}{\mu_1} \tag{27}$$

Energy loss in the disc plate is caused by the working fluid rotating in the space between the annular-shaped surface of the rear shroud and the side wall of the compressor housing. The surface area of this annulus in the rear shroud is determined by integrating between the radius of the hub (r_i) and the circumference (r_{IMP}) of the impeller as shown in equation (28).

$$W'_{disk} = \frac{1}{\dot{m}} \pi \rho f_{disk} \omega^3 \int_{r_i}^{r_{IMP}} r^4 dr = \frac{1}{\dot{m}} \left\{ \frac{\pi \rho f_{disk} \omega^3 \left(r_{IMP}^5 - r_i^5\right)}{5} \right\} \tag{28}$$

Energy loss of a fluid rotating on a curved surface of a frustum (W''_{disk}) shown in equation (29) is approximate to the actual disk friction loss due to local friction between the working fluid and the curved surface of the impeller running frontally from the hub to the circumference.

$$W''_{disk} = \frac{1}{\dot{m}} \omega r_{ave} \left(\tau A_{curv}\right) = \frac{1}{\dot{m}} \left\{ \frac{\rho f_{curv} \omega^3 r_{ave}^3 A_{curv}}{2} \right\} \tag{29}$$

Unlike the case of the disc plate, the radius of the conical frustum is obtained by averaging rather than integration to avoid unnecessary complexities as shown in equation (30).

$$r_{ave} = \frac{r_{IMP} + r_i}{2} \tag{30}$$

The curved surface area of the frustum (A_{curv}) is:

$$A_{curv} = \pi \left(r_{IMP} + r_i\right) \cdot \sqrt{\left(r_{IMP} - r_i\right)^2 + H_{IMP}^2} \tag{31}$$

The local friction factor corresponding to shear stresses on the smooth curved surface is:

$$f_{curv} = 0.046 \left(\mathrm{Re}\right)_{curv}^{0.20} \tag{32}$$

The approximate Reynolds Number (Re_{curv}) for the curved surface of the frustum is:

$$\mathrm{Re}_{curv} \approx \frac{\rho_2 U_2 \left\{D_{IMP} - d_i + \left(2 \cdot Gap\right)\right\}}{\mu_1} \tag{33}$$

3.2.3.2 Leakage Losses

The difference between the inlet and outlet pressures generated in the compressor causes a portion of the working fluid flowing in the direction of the discharge port to return to the inlet port through the clearance between the impeller's circumference and the compressor housing. The backflow of some of the fluid means that the centrifugal machine's actual delivery capacity is

usually lower than its theoretical capacity. Leakage is a contributor to the overall energy losses in centrifugal machines.

$$W_{leak} = \frac{1}{\dot{m}} \left\{ \frac{2\dot{m}_{gap}\Delta P_{gap}}{\rho_2} \right\} \tag{34}$$

$$\Delta P_{gap} = \frac{\dot{m}\left(r_{IMP} \cdot V_{t2} - r_m \cdot V_{t1}\right)}{n_B \cdot \left(\frac{r_{IMP} + r_m}{2}\right) \cdot \left(\frac{b_1 + b_2}{2}\right) \cdot L_{IMP}} \tag{35}$$

As show in equation (34), energy loss due to leakage (W_{leak}) is strongly influenced by leakage mass flow rate ($\dot{m}_{gap}$) and the differential pressure across the clearance (ΔP_{gap}). The actual mass flow rate of fluid flowing out of the compressor discharge port is represented by ($\dot{m}$).

$$\dot{m}_{gap} = \rho_2 \cdot n_B \cdot L_{IMP} \cdot Gap \cdot V_{gap} \tag{36}$$

The leakage mass flow rate is a function of the fluid density, leakage velocity (V_{gap}), number of impeller blades (n_B) and flow area of the clearance. The clearance is assumed to be rectangular in shape. Therefore, its flow area is the product of the width of the clearance (*Gap*) and the length of the impeller blades (L_{IMP}).

$$V_{gap} = \frac{1}{1 - K_{loss}} \cdot \sqrt{\frac{\Delta P_{gap}}{\rho_2}} \tag{37}$$

$$K_{loss} = \frac{1}{2}\left(\frac{\mathrm{Gap}}{\mathrm{b}_1 + \mathrm{Gap}} + \frac{\mathrm{Gap}}{\mathrm{b}_2 + \mathrm{Gap}}\right) \tag{38}$$

The loss coefficient (K_{loss}) describes the fraction of the working fluid back-flowing through pathways created by the clearance area between the compressor housing and the impeller's leading and trailing edges.

3.2.3.3 Hydraulic Losses

Hydraulic losses are energy losses associated with the flow of the working fluid through the blade channels running from the impeller's eye to its circumference. Energy losses in the diffuser and volute are also included. Hydraulic losses are quite distinct from leakage losses. The former refers losses incurred as the working fluid flows from inlet to outlet of the compressor while the latter refers to losses incurred when a portion of the working fluid flowing towards the outlet turns around and returns to the inlet via the clearances.

Hydraulic losses are generated in four ways:

- skin friction generated as the working fluid flows through blade channels with the impeller
- shock losses due to change in the flow path of the working fluid from axial to radial direction (see Fig. 2)
- losses due to gradual contraction of the flow area from the inlet to the outlet
- sudden deceleration of the working fluid in the diffuser and volute of the compressor

For the purposes of this study, only the first three sources of hydraulic losses in the centrifugal compressor are modelled.

$$W_{HYD} = 2f_{HYD}\mathrm{V}^2_{\mathrm{rel,\ ave}}\left(\frac{L_{IMP}}{D_{HYD}}\right) + \frac{K_{sum}\mathrm{V}^2_{\mathrm{rel1}}}{2} \tag{39}$$

The first term in equation (35) describes energy loss due to skin friction between the working fluid and the walls of the blade channels in which it is flowing. The second term describes losses due to change in the flow direction and losses due to the gradual contraction of the flow area of the blade channels from the leading to trailing edge of the impeller.
The shear stress developed on the walls of the blade channels carrying the working fluid is dependent on the local friction factor (f_{HYD}); mean relative velocity ($\mathrm{V}_{\mathrm{rel,ave}}$); the length ($L_{IMP}$) and hydraulic diameter (D_{HYD}) of the blade channels. The mentioned parameters are presented in equations (40) to (45).

$$f_{HYD} = 0.046\left(\mathrm{Re}\right)^{0.20}_{HYD} \tag{40}$$

$$\mathrm{Re}_{HYD} \approx \frac{\rho_2 \cdot \mathrm{V}_{\mathrm{rel,\ ave}} \cdot D_{HYD}}{\mu_1} \tag{41}$$

$$\mathrm{V}_{\mathrm{rel,\ ave}} = \sqrt{\frac{\mathrm{V}^2_{\mathrm{rel1}} + \mathrm{V}^2_{\mathrm{rel2}}}{2}} \tag{42}$$

The hydraulic diameter proposed by Boyce [38] for the blade channels was used:

$$D_{HYD} = \frac{2\left(A_1 \cos\beta_1\right)}{\left\{\pi \cdot \left(d_o + d_i\right) \cdot \cos\beta_1\right\} + \left\{2 \cdot n_B \cdot \left(d_o - d_i\right)\right\}} + \frac{\left(A_2 \cos\beta_2\right)}{\left\{\pi \cdot D_{IMP} \cdot \cos\beta_2\right\} + \left\{n_B \cdot b_2\right\}} \tag{43}$$

The length of the blade channels (L_{IMP}) was is a function of the meridional length (L_m) and the impeller's blade angle (β):

$$L_{IMP} = \frac{L_m}{\sin\beta} \tag{44}$$

Where,

$$L_m = \tan\beta \cdot \left(\frac{r_{IMP} + r_m}{2}\right) \cdot \theta \;=\; \tan\beta \cdot \left(\frac{r_{IMP} + r_m}{2}\right) \cdot \left(\frac{2\pi}{n_B}\right) \tag{45}$$

From Fig.2, it is clear that the profile of blade channel resembles a combination of a pipe elbow and a contracting pipe cross-section. Therefore, the second term in equation (35) was modelled using the sum of loss coefficients for a pipe elbow (K_{curv}) and gradual contraction of a pipe (K_{con}) as shown below:

$$K_{sum} = K_{curv} + K_{con} \tag{46}$$

The loss coefficient for gradual contraction (K_{con}) is based on the Crane [40] correlation:

$$K_{con} = \begin{cases} 0.8\left(1 - \dfrac{A_2}{A_1}\right) \cdot \sin\left(\dfrac{\phi}{2}\right) & \text{for } \phi \le 45\,\text{deg} \\ 0.5\left(1 - \dfrac{A_2}{A_1}\right) \cdot \sqrt{\sin\left(\dfrac{\phi}{2}\right)} & \text{for } 45\ \text{deg} \le \phi \le 180\ \text{deg} \end{cases} \tag{47}$$

3.3 Set-up for the study of compressor performance

3.3.1 Compressor Type

The single-stage centrifugal machine used in this study is unrealistically small for an actual CO_2 transport pipeline. Its maximum delivery capacity (i.e. highest flow rate it can muster) is only a small percentage (2%–20%) of typical flow rates of the CO_2 stream. Moreover, centrifugal compressors used in transport pipelines are typically multi-staged rather than single-staged. The decision to use this small sized centrifugal compressor in this study was made because experimental data for a real-life machine of the same type and size was conveniently available for model validation.

Due to geometric and dynamic similarities, the performance analysis of the small compressor can be scaled up to apply to larger compressors relevant to CCS transport, provided affinity laws are applied to centrifugal machines handling pure CO_2 or an impure CO_2 stream of identical composition under the same operating conditions.

3.3.2 Composition of the carbon dioxide-based working fluids

For the purposes of this study, pure CO_2 and CO_2 in binary mixtures with N_2, H_2, CO and CH_4 were selected as the working fluids of the compressor. For the impure CO_2 mixtures, two sets of scenarios have been created. In one set, the purity of the CO_2 in the mixture has been fixed at 90% by mole while in the other set, CO_2 purity is fixed at 80% by mole. Obviously, the concentration of impurities in the working fluids used in this study is too high to be reflective of CO_2 streams expected in an actual CO_2 transport pipeline. They have been selected primarily to study the effect of each type of impurity on compressor performance as well as the impact of rotor sizing and rotor speed on energy requirement of the machine.

3.3.3 Compressor design parameters and operational conditions

Tables 1 and 2 presents the input design parameters and operational conditions of the small-sized compressor used in this study. Most, but not all, the design input parameters used were culled from the experimental work conducted by Aritomi et al. [25].

Table 1. Design parameters of a centrifugal compressor simulated with proposed model.

Compressor Geometry	Dimensions
Impeller diameter	76.00 mm
Impeller blade height	20.40 mm
Number of impeller blades	16
Inlet diameter at the root of impeller eye	19.94 mm
Inlet diameter at the tip of impeller eye	40.00 mm
Outflow depth (i.e. impeller width at trail edge)	3.42 mm
Impeller blade angle	70.00 deg.
Rotor shaft diameter	68.00 mm
Rotor shaft length	560.00 mm

The input operational conditions shown in Table 2 are exactly the same as those used in Aritomi et al. [25].

Table 2. Input conditions of a centrifugal compressor simulated with proposed model.

Operating Condition	Range
Mass flow rate ($\dot{m}$)	2.242 – 4.008 kg/s
Rotor speed (N)	8298 – 14310 rpm
Inlet pressure (P_1)	75.88 – 82.71 bar
Inlet temperature (T1)	308.30 – 310.60 K

This is particularly important because the authors provided experimental output data on a real-life compressor of identical small size, which is perfect for the validation of the proposed model.

3.4 Validation of Model

As is the case with many CCS research work, only a limited amount of experimental or real plant data are available in the public domain. The authors of this work have not seen any published experimental performance data for single-stage centrifugal compressors or pumps operating in the context of CCS transport under supercritical conditions. For this reason, we turned to published studies in the field of nuclear power such as [23, 24, 25, 34] which report on centrifugal compressors used in experimental rigs running on the supercritical CO_2 Brayton cycle. Compressors used in supercritical CO_2 Brayton cycle are much smaller in size and have a delivery capacity that is only a fraction of what obtains in CO_2 transport pipelines used in CCS schemes. However, these small compressors operate at very high pressures and temperatures comparable with what obtains in CO_2 pipeline transportation.

Table 3. Validation of proposed model using experimental compressor data for pure CO_2 condition

N	M	P_1	T_1	Outlet Pressure (bar)			Outlet Temperature (K)		
rpm	kg/s	bar	K	Experiment	Prediction	Error (%)	Experiment	Prediction	Error (%)

8298	2.24	76.08	308.50	78.10	78.37	0.34	310.10	310.44	0.11
10104	2.73	77.43	309.90	80.39	80.81	0.53	312.30	312.75	0.14
10704	2.89	77.63	310.10	80.94	81.43	0.60	312.70	313.27	0.18
11298	3.06	77.98	310.40	81.68	82.23	0.68	313.30	313.90	0.19
11904	3.22	77.91	310.40	82.01	82.61	0.74	313.70	314.26	0.18
12000	4.01	82.71	308.50	91.34	91.76	0.46	311.50	312.39	0.29
12498	3.39	77.74	310.20	82.25	82.93	0.82	313.90	314.46	0.18
13103	3.74	76.21	308.30	81.41	82.02	0.75	312.30	313.04	0.24
13111	3.55	77.86	310.40	82.81	83.55	0.89	314.40	315.05	0.21
13704	3.92	77.06	309.20	82.76	83.39	0.76	313.50	314.36	0.27
13710	3.72	77.97	310.60	83.38	84.17	0.94	314.90	315.64	0.24
14310	3.88	75.88	308.60	81.75	82.57	1.00	313.30	314.15	0.27

All supercritical CO_2 Brayton cycle test rigs circulate pure CO_2 as the working fluid. Therefore, the proposed model was validated only for the condition of a compressor handling a pure CO_2 stream using experimental data from [25]. As presented on Table 3, the proposed model is quite robust with a maximum relative error of just 1.0%. The model could not be validated for the condition of a compressor handling impure CO_2 due to the lack of experimental performance data.

4. Analysis of Compressor Performance

4.1 Effect of impurities on compressor performance

Centrifugal compressors function by using impellers spinning at a high speed (N) to impact momentum tangentially to the working fluid flowing into the machine through the inlet port. In the diffuser (near the outlet duct) of the compressor, the fluid flowing at high speed decelerates due to flow resistance in the passages of the pump's diffuser and converts to pressure in accordance with Bernoulli's Principle. In other words, the outlet pressure (P_2) is a function of the density and the velocity of the working fluid. As shown in Figs. 3(a) and 3(b), for a given working fluid, an increase in the rotor speed (N) will develop a corresponding higher pressure in the compressor's discharge port.

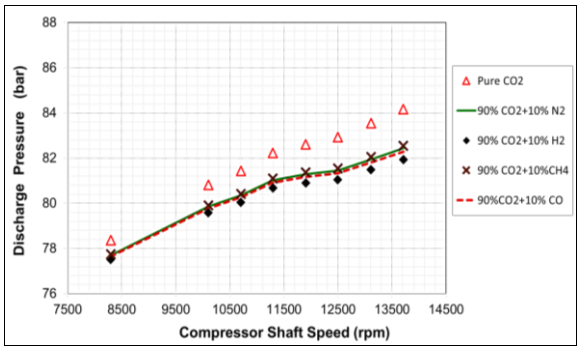

Fig.3(a). Effect of impurities on outlet pressure for 90% CO_2 purity

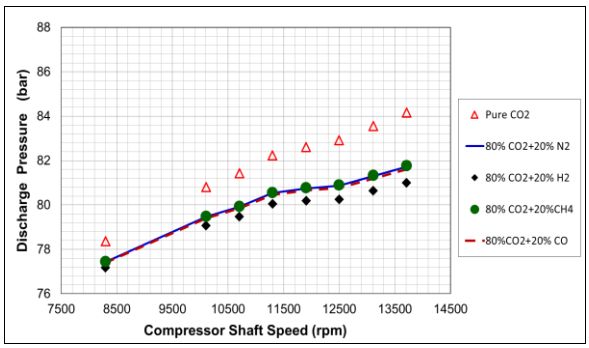

Fig.3(b). Effect of impurities on outlet pressure for 80% CO_2 purity

The impurities featured in this study namely N_2, H_2, CH_4 and CO all have lower molecular weights than carbon dioxide. As shown in Fig. 1(b), their introduction into the carbon dioxide stream have the effect of reducing the overall density which will immediately result in the decline of the fluid angular momentum developed from the torque of the compressor rotor shaft. Reduction in fluid angular momentum will lead to degradation of the discharge

pressure head. These impurities also increase energy losses resulting in the reduction in the isentropic efficiency.

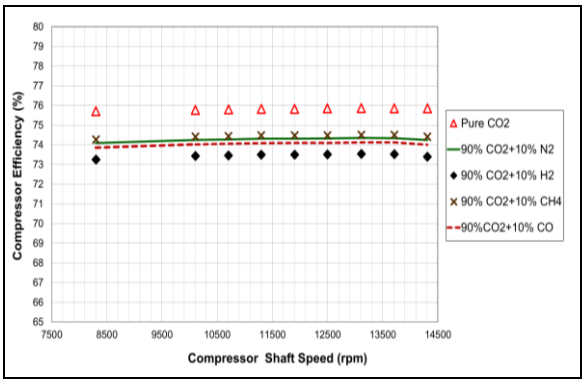

Fig. 4(a). Effect of impurities on efficiency for 90% CO_2 purity

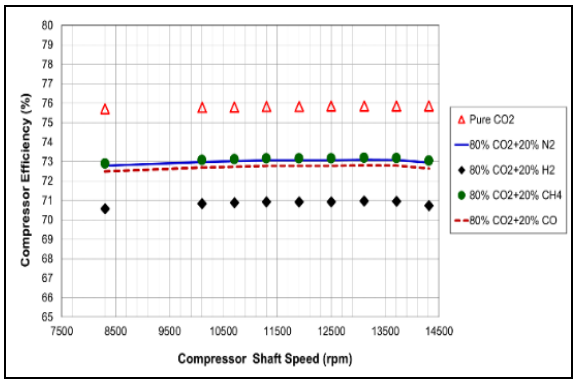

Fig. 4(b). Effect of impurities on outlet pressure for 80% CO_2 purity

The severity of the degradation of the compressor performance depends on the type and concentration of the impurity in the CO_2 stream flowing in the machine. From Figs. 3 and 6, it is clear that for a given rotor speed, the hydrogen impurity in the CO_2 causes the greatest reduction in the outlet pressure (P_2) built up in the compressor diffuser. At the same time, because of large energy losses, the energy requirement of the compressor is highest while isentropic efficiency is lowest (See Figs. 4 and 5). All these can be attributed to the drastic reduction in the overall fluid density because sharp contrast between molar mass of hydrogen (2.016 g/mol.) and that of carbon dioxide (44.01 g/mol.). The other impurities, nitrogen, methane and carbon monoxide, have higher molar masses than hydrogen and therefore their effect on compressor performance are less severe. Comparing Figs. 3(a) to 3(b) and Figs. 4(a) to 4(b), it is observed that increasing the concentration of the impurities in the carbon dioxide-based working fluids from 10% to 20%, has the effect of further degradation in compressor performance. However, it should be noted that for a given working fluid, the isentropic efficiency barely changes with increasing compressor shaft speed (N). This is in contrast to the discharge pressure which varies with changing shaft speed (N). Since compressor efficiency barely changes with shaft speed, it is quite reasonable to use averaged efficiency values as a measure of compressor performance for each of the working fluids as shown in Fig.5.

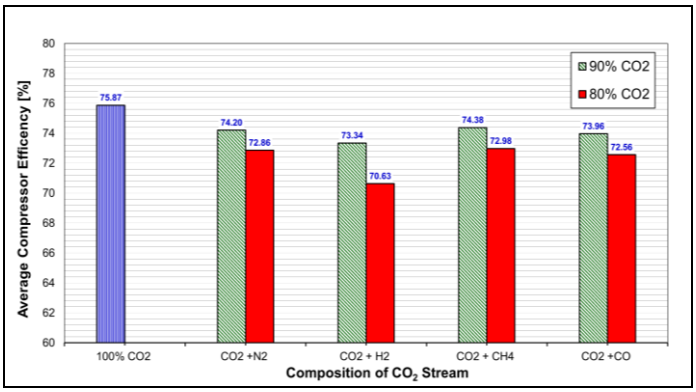

Fig.5. Average isentropic efficiency for working fluids with 80%, 90% and 100% CO_2 purity

As shown in Table 1, for all working fluids regardless of composition, the input operating conditions for the proposed compressor model are the same. This was done to allow for a parametric study of the effect of introducing and altering the concentration of the impurities.

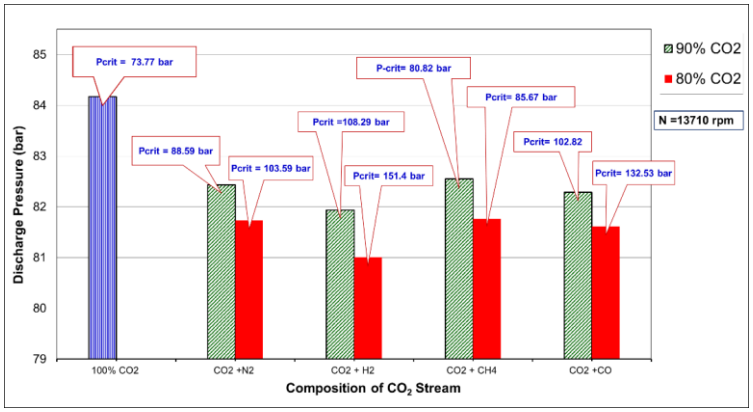

Fig.6. Compressor discharge pressures for different working fluids with their critical pressures

However, using the same input conditions have the effect of generating discharge pressures that are sufficiently above the critical point to keep only pure CO_2 and CO_2/CH_4 mixed streams in the supercritical phase prescribed for long distance CO_2 pipeline transport. The other mixed CO_2 streams flow out of the compressor's outlet port in gaseous phase because the discharge pressures generated are below their critical pressures.

As illustrated in Fig.6, the shifting nature of the critical pressure (P_{crit}) depending on type and concentration of the impurity in a CO_2 stream means that the discharges pressure (P_2) will have to be raised far above the critical pressure (P_{crit}) of each working fluid. This will ensure that the working fluids are in the supercritical phase prior to introduction into the transport pipeline.

4.2 Compressor energy requirement— rotor sizing versus rotor speed adjustment

In a centrifugal compressor, the discharge pressure (P_2) can be raised either by increasing the shaft speed (N) or enlarging the diameter of the impeller. These methods of increasing the discharge pressure will have different consequences for the energy losses incurred as a result. As shown in Fig. 9, increasing the shaft speed while machine size remains unchanged will generate far more energy losses than vice-versa. In other words, increasing shaft speed to generate a particular discharge pressure will require more work input (W_{INPUT}) than if the machine size was proportionally increased while the shaft speed remained constant (See Fig. 8).

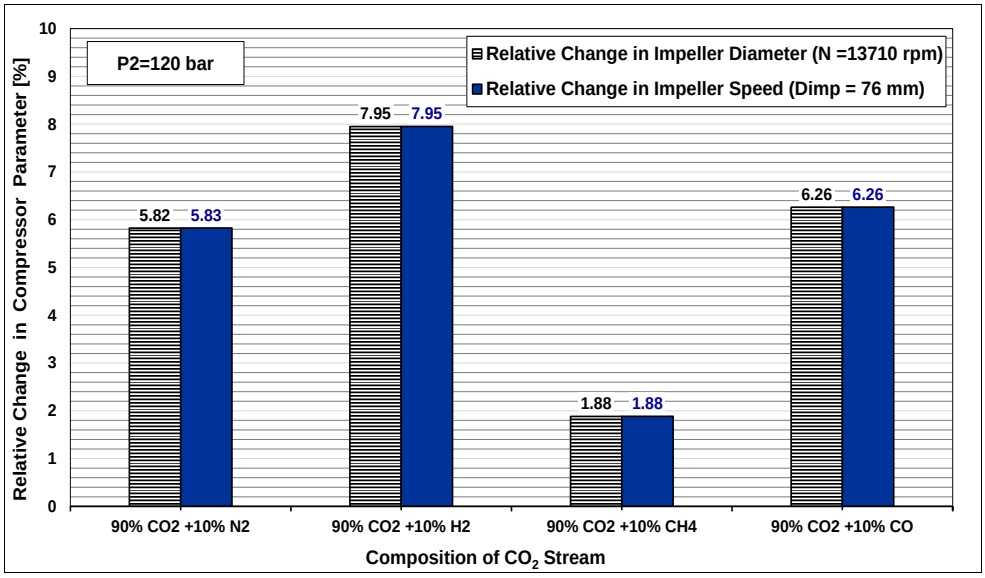

Fig.7. Relative change in impeller size versus relative change in impeller speed for different CO_2 streams

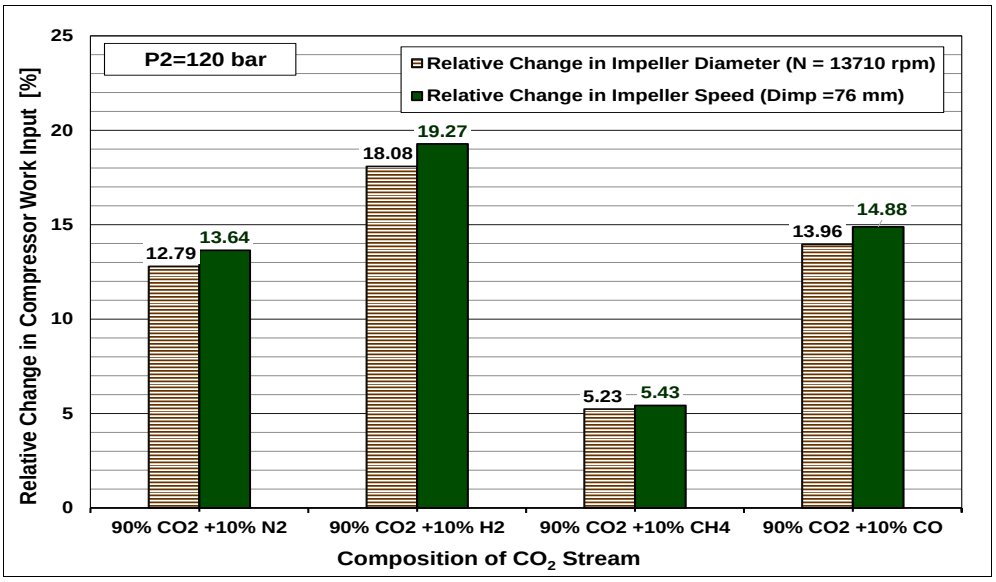

Fig.8. Effect of impeller size versus effect of impeller speed on compressor work input for different CO_2 streams

In this section, the effect of rotor sizing on work input was investigated and compared to the effect of rotor speed on work input using only working fluids with CO_2 purity of 90% and 100%. From Fig.6, it can be observed that the critical pressure of the five selected working fluids range from 73.77 bar to 108.29 bar. At shaft speed of 13710 rpm, only the pure CO_2 and CO_2/CH_4 mixture were sufficiently pressurized to flow out of the discharge port as supercritical fluids. In the remaining three cases—CO_2/N_2, CO_2/H_2 and CO_2/CO mixtures—the discharge pressures (P_2) was below their individual critical pressures (P_{crit}) causing them to emerge from the compressor's outlet port in gaseous state. To ensure that all selected working fluids flow out of the compressor in supercritical phase, a standard outlet pressure (P_2) of 120 bar was chosen.

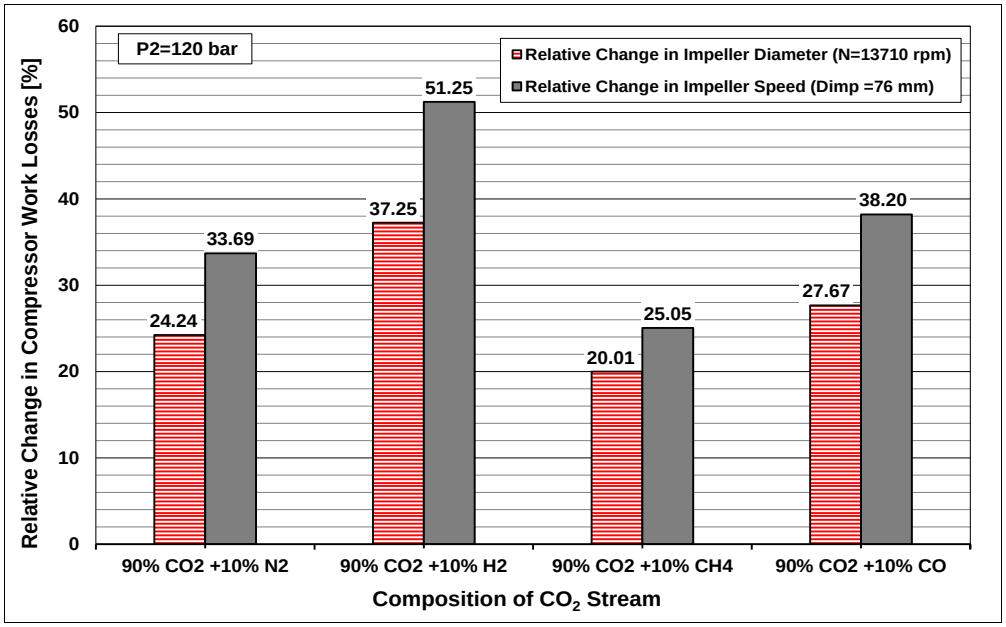

Fig.9. Effect of impeller size versus effect of impeller speed on compressor energy losses for different CO_2 streams

Therefore, for each of the 5 selected working fluids, rotor size, rotor speed and work input required to raise the compressor discharge pressure to 120 bar was calculated. Relative changes in compressor size, rotor speed, work input and energy losses shown in Figs. 7 to 9, are percentage differences used as a method of evaluating how the increase in P_2 affects the diameter and speed of the impeller and energy requirement for a compressor handling each of the selected CO_2 mixtures compared to one handling pure CO_2.

From Fig. 1(b), it can be observed that for a given temperature and pressure, the fluid density progressively decreases as working fluid changes from pure CO_2 to CO_2/CH_4, CO_2/N_2, CO_2/CO and finally, CO_2/H_2 mixtures. Therefore, it is not surprising that a compressor handling the CO_2/H_2 working fluid—the least dense mixture— will require the highest amount of energy (W_{INPUT}) to generate the stipulated outlet pressure of 120 bar. After all, compression work input is inversely proportional to fluid density. For a constant shaft speed of 13710 rpm, this energy requirement will translate to the largest compressor re-sizing effort. In relative terms, the compressor size will increase by 7.95% and work input will increase by 18.08% as shown in Figs. 7 and 8 when the compressor shifts from handling pure CO_2 to CO_2/H_2 mixture. Alternatively, if the compressor rotor size was left unchanged at 76mm, the rotor speed will increase by exactly the same 7.95% as the working fluid shifts from pure CO_2 to CO_2/H_2 mixture. However, the energy requirement (W_{INPUT}) will jump to 19.27%. The reason for all this can be found in Fig.9 where the rotor re-sizing effort results in a relative change in energy loss of 37.25% compared to a whopping 51.25% for rotor speed adjustment.

The CO_2/CH_4 mixture, with the second highest density values after those of pure CO_2, requires the least amount of energy and the least compressor re-sizing and speed regulation effort. At 13710 rpm, the rotor size will increase by 1.88% and the work input will increase by 5.23% when compressor shifts from handling pure CO_2 to CO_2/CH_4 mixture (See Figs.7 and 8). Alternatively, if the rotor size is maintained at 76mm, the rotor speed will increase by the same 1.88% and the work input will rise by 5.43% when working fluid shifts from pure CO_2 to

CO_2/CH_4 mixture. As shown in Fig.9, the relative change in energy loss incurred for the rotor re-sizing effort is 20.01% compared to 25.05% incurred for the rotor speed regulation effort.

So generally speaking, discharge pressure, rotor speed, rotor size and work input are in a directly proportional relationship. That relationship is inversely proportional to the overall fluid density which in turn is dependent on the composition of the carbon dioxide-based working fluid. It is important to reiterate that for the same discharge pressure, energy losses incurred as a result of increasing the rotor speed while keeping compressor size constant is greater than energy losses associated with increasing the size of the rotor while keeping compressor speed constant.

5. Conclusions

A quasi-dimensional model, governed by the laws of conservation, has been developed to study and compare the effect of re-sizing the rotor against the effect of adjusting the rotor speed on energy requirement of a centrifugal compressor handling supercritical CO_2 either in pure form or in binary mixtures with different chemical impurities.

The proposed model— validated with available experimental data on pure CO_2— differs from previous compressor models in that it includes detailed information on machine geometry which means it can potentially be used to optimize the procedure for compressor sizing and selection. Compressor performance curves which have traditionally being used for this purpose is unsuitable in the CCS context as none have been developed for relevant carbon-dioxide based working fluids flowing at supercritical or dense phase conditions.

From the preliminary study carried out with this model, it was noted that in centrifugal compressors, the discharge pressure is a function of density and the velocity of the working fluid. Impurities in the CO_2 stream have a strong effect on overall fluid density, reaffirming what many other researchers have reported in their published works. Impurities reduce the overall fluid density causing the discharge pressure to drop, in most cases, below the critical pressures of the working fluids. To raise the discharge pressure, the compressor shaft speed will either have to be increased or the machine can be re-sized while shaft speed remains constant. Either way, an increase in energy requirement is the penalty that must be paid for the discharge pressure to be upwardly adjusted. However, compressor re-sizing is preferable to increasing compressor shaft speed because the latter incurs more energy losses than the former. Compressor re-sizing is directly proportional to energy requirement which in turn is inversely proportional to fluid density. Therefore, the type and concentration of the impurity in the working fluid plays a big role in deciding the optimal size of the compressor which will give the best attainable efficiency per power utilized and reduce energy penalty and operating costs in a CO_2 transport pipeline network.

References

[1] Svensson, R., Odenberger, M., Johnsson,F. and Stromberg, L., 2004. “Transportation systems for CO2—application to carbon capture and storage”. Energy Conversion and Management, Vol.45, pp. 2343–2353

[2] Zhang, Z.X., Wang, G.X., Massaroto, P. and Rudolph, V., 2006. Optimization of pipeline transport for CO2 sequestration. Energy Conversion and Management, Vol.47, pp.702–715.

[3] Lazic, T., Oko, E. and Wang, M., 2014. Case study on CO2 transport pipeline network design for Humber region in the UK. Proc IMechE Part E: Journal of Process Mechanical Engineering, Vol. 228(3) 210–225

[4] Luo, X., Wang, M., Oko, E. and Okezue, C. Simulation-based techno-economic evaluation for optimal design of CO2 transport pipeline network. *Applied Energy*, Vol. 132, pp. 610–620.

[5] Adams, R., 2011. “CO2 Capture and Pumping”. Proceedings of the Twenty-Seventh International Pump User Symposium, Houston, Texas, USA.

[6] Li, H. and Yan, J., 2009. “Impacts of equations of state (EOS) and impurities on the volume calculation of CO2 mixtures in the applications of CO2 capture and storage (CCS) processes”. Applied Energy, Vol. 86, pp. 2760–70
[7] Oosterkamp, A. and Ramsen, J., 2008. “State of the Art Review of CO2 Pipeline Transport with Relevance to Offshore Pipelines”. Report No. POL-0-2007-138-A, Polytec, Norway.
[8] Seevam, P.N., Race, J.M., Downie, M.J. and Hopkins, P., 2008. “Transporting the Next Generation of CO2 for Carbon Capture and Storage: The Impact of Impurities on Supercritical CO2 Pipelines”. Proceedings of 7th International Pipeline Conference, Calgary, Alberta, Canada.
[9] Seevam, P.N., Race, J.M., Downie, M.J., Barnett, J. and Cooper, R., 2010. “Capturing Carbon dioxide: The Feasibility of Re-Using Existing Pipeline Infrastructure to Transport Anthropogenic CO2”. Proceedings of the 8th International Pipeline Conference, Calgary, Alberta, Canada
[10] Goos, E., Riedel, U., Zhao,L. and Blum,L., 2011. “Phase diagrams of CO2 and CO2-N2 gas mixtures and their application in compression processes”. Energy Procedia, Vol.4, pp. 3778-3785
[11] Wetenhall, B., Aghajani, H., Chalmers, H., Benson, S.D., Ferrari, M-C., Li, J., Race, J.M., Singh and P., Davison, J.,2014. “Impact of CO2 impurity on CO2 compression, liquefaction and transportation”. Energy Procedia, Vol.63, pp.2764-2778
[12] Race, J., Wetenhall, B., Seevam, P. and Downie, M., 2012. “Towards a CO2 pipeline specification: defining tolerance limits for impurities”. Journal of Pipeline Engineering, Vol.11, No. 3, 2012, pp. 173-189
[13] Eickhoff, C., Neele, F., Hammer, M., DiBiagio, M., Hofstee, C., Koenen, M., Fischer, S., Isaenko, A., Brown, A. and Kovacs, T., 2014. “IMPACTS: economic trade-offs for CO2 impurity specification”. Energy Procedia, Vol. 63, pp. 7379 – 7388
[14] Nimtz, M., Klatt, M., Bernd, W., Kuhn, M. and Krautz, H.J., 2010. “Modelling of the CO2 process- and transport chain in CCS systems—Examination of transport and storage processes”. Chemie der Erde, Vol. 70, Supplement 3, pp. 185-192
[15] Chaczykowski, M. and Osiadacz, A. J., 2012. “Dynamic simulation of pipelines containing dense phase/supercritical CO2-rich mixtures for carbon capture and storage”. International Journal of Greenhouse Gas Control, Vol. 9, pp. 446-456.
[16] Liljemark, S., Arvidsson, K., McCann, M.T.P., Tummescheit, H. and Velut, S., 2011. “Dynamic simulation of a carbon dioxide transfer pipeline for analysis of normal operation and failure modes”. Energy Procedia, Vol. 4, pp. 3040-3047.
[17] Aursand, P., Hammer, M., Munkejord and Wilhelmsen, Ø., 2013. “Pipeline transport of CO2 mixtures: Models for transient simulation”. International Journal of Greenhouse Gas Control, Vol. 15, pp. 174-185.
[18] Brown, S., Mahgerefteh, H., Martynov, S., Sundara, V. and MacDowell, N., 2015. “A multi-source flow model for CCS pipeline transport networks”. International Journal of Greenhouse Gas Control, Vol.43, pp.108-114
[19] Witkowski, A., Rusin, A., Majkut, M., Rulik, S. and Stolecka, K., 2013. “Comprehensive analysis of pipeline transportation systems for CO2 sequestration: Thermodynamics and safety problems”. Energy Conversion and Management, Vol. 76, pp. 665-673.
[20] Martynov,S.B., Daud,N.K., Mahgerefteh, H., Brown, S., Porter, R.T.J., 2016. “Impact of stream impurities on compressor power requirements for CO2 pipeline transportation”. International Journal of Greenhouse Gas Control, Vol.54, pp.652-661.
[21] Okezue, C. and Wang, M., 2016. “Performance Evaluation of a Pump Used For CO2 Transport”. 11th European Conference on Coal Research and Its Applications, Sheffield, United Kingdom.
[22] Moore, J.J., Lerche, A., Delgado, H., Allison, T. and Pacheco, J., 2011. “Development of Advanced Centrifugal Compressors and Pumps for Carbon Capture and Sequestration Applications”. Proceedings of the 40th Turbomachinery Symposium, Houston, Texas
[23] Wright, S.A., Pickard, P.S., Vernon, M.E. and Radel, R.F., 2009. “Description and Test Results from a Supercritical CO2 Brayton Cycle Development Program”. 7th International Energy Conversion Engineering Conference, Denver, Colorado, USA.
[24] Lee, J., Kim, S.G., Cha, J.E., Lee, J.I., 2014. “Uncertainty on Performance Measurement of Supercritical CO2 Compressor Operating Near Critical Point”. 4th International Symposium - Supercritical CO2 Power Cycles, Pittsburgh, Pennsylvania
[25] Aritomi, M., Ishizuka T., Muto, Y and Tsuzuki, N., 2011. “Performance Test Results of a Supercritical CO2 Compressor Used In a New Gas Turbine Generating System”. Journal of Power and Energy Systems, Vol.5, No.1, pp. 45-59
[26] Li, H., Wilhelmsen,Ø., Lv, Y., Yan, J., 2011. “Viscosities, thermal conductivities and diffusion coefficients of CO2 mixtures: Review of experimental data and theoretical models”. International Journal of Greenhouse Gas Control, Vol.5, pp.1119-1139
[27] Wilhelmsen, Ø., Skaugen, G., Jørstad O. and Li, H. 2012. “Evaluation of SPUNG and other Equations of State for use in Carbon Capture and Storage modelling”. Energy Procedia, Vol. 23, pp. 236-245
[28] Wadas, B., 2010. “Compression and Pumping Technologies and Experience for EOR/CCS Applications”.CO2 Summit: Technology and Opportunity, Engineering Conferences International, Colorado, USA
[29] Demetriades, T.A., Drage, T.C. and Graham, R.C., 2013. “Developing a new equation of state for carbon capture and storage pipeline transport”. Journal of Process Mechanical Engineering, Volume 227, Issue No 2, pp 117-124
[30] Diamantonis, N.I., Boulougouris, G.C., Mansoor, E., Tsangaris, D.M., Economou, I.G., 2013. “Evaluation of Cubic, SAFT and PC-SAFT Equations of State for the Vapour-Liquid Equilibrium Modelling of CO2 Mixtures with Other Gases”. Industrial & Engineering Chemistry Research, American Chemical Society, Vol.52, pp.3933-3942
[31] Demetriades,T.A. and Graham, R.S., 2016. “A new equation of state for CCS Pipeline Transport: Calibration of mixing rules for binary mixtures of CO2 with N2, O2 and H2”. Journal of Chemical Thermodynamics, Vol. 93, pp. 294-304
[32] Ramos, A., Calado, M., Dias, E., Lawal, A., Rodriguez, J., Samsatli, N., Sanchis, G., Matzopoulos, M. and Pantelides, C., 2014. “CCS System Modelling and Simulation”. 4th Korean CCS Conference, Jeju Island, Korea
[33] Kunz, O., Wagner, W., 2012. “The GERG-2008 wide-range equation of state for natural gases and other mixtures: an expansion of GERG-2004”. J Chem Eng Data, Vol.57, Issue 11, pp.3032–91.
[34] Lee, J., Baik, S., Cho, S.K., Cha, J.E., Lee, J.I., 2016. “Issues in performance measurement of CO2 compressor near the critical point”. Applied Thermal Engineering, Vol.94, pp 111-121
[35] Stodola, A., 1927. Steam and gas turbines. Volumes I and II. McGraw-Hill, New York, USA.
[36] Saravanamutto, H.I.H, Roger, G.F.C. and Cohen, H., 2001. Gas turbine theory (5th Edition). Pearson Education Limited, Essex, UK
[37] Douglas, J.F., Gasiorek, J.M., Swaffield, J.A. and Jack, L.B., 2005. Fluid Mechanics (5th Edition). Pearson Education Limited, UK
[38] Boyce, M.P., 1972. “New developments in compressor aerodynamics”. Proceedings of the First Turbomachinery Symposium, Texas, USA, pp.79-89
[39] Martynov, S., Mahgerefteh, H., Brown, S., 2012. “CO2 Transportation for CCS”. Powerpoint Presentation at UKCCS Winter School at University of Cambridge, UK
[40] Crane Company, 1982. “Flow of Fluids through Valves, Fittings, and Pipe”. Technical Paper No. 410 M.